Journal of Photochemistry and Photobiology B: Biology 115 (2012) 85–92

Contents lists available at SciVerse ScienceDirect

Journal of Photochemistry and Photobiology B: Biology

journal homepage: www.elsevier.com/locate/jphotobiol

Antioxidant benzimidazole bind bovine serum albumin

J. Jayabharathi *, V. Thanikachalam, K. Jayamoorthy

Department of Chemistry, Annamalai University, Annamalainagar, Tamilnadu 608 002, India

ARTICLE INFO

Article history:
Received 4 June 2012
Received in revised form 26 June 2012
Accepted 30 June 2012
Available online 11 July 2012

Keywords:
Antioxidant
Benzimidazole
BSA
Quenching
FRET

ABSTRACT

1-(4-Methoxybenzyl)-2-(4-methoxyphenyl)-1H-benzo[d]imidazole (MBMPB) was synthesized and characterized by ^{1}H NMR, ^{13}C NMR, Mass and IR spectral analysis. The mutual interaction of MBMPB with bovine serum albumin (BSA) was investigated using solution spectral studies. The binding distance has been calculated based on the theory of Forester's non-radiation energy transfer (FRET). The Stern–Volmer quenching constant (K_{sv}) were calculated at different temperature. The binding site (n), apparent binding constant (K_A) and corresponding thermodynamic parameters ($\Delta G, \Delta H$ and ΔS) were calculated. Antioxidant analyses such as DPPH radical scavenging analysis, Superoxide anion scavenging analysis and Hydroxyl radical scavenging analysis have been carried out for MBMPB and it shows potential antioxidant property due to the presence of electron releasing methoxy group.

© 2012 Elsevier B.V. All rights reserved.

1. Introduction

Fused imidazole derivatives such as benzoimidazoles and phenanthroimidazoles [1–3] have been used in the fabrication of light-emitting devices, employing them as electron-transporting layer and as sensitizers in dye-sensitized solar cells [4,5] due to their wide optical absorption, bright luminescence and bipolar transport characteristics. Imidazole nucleus forms an important structure of human organisms, i.e., the amino acid histidine, vitamin B_{12}, a component of DNA base structure and also has significant analytical applications utilizing their fluorescence and chemiluminescence properties [6].

Free radicals, the partially reduced metabolites of oxygen and nitrogen, are highly toxic and reactive. Free radicals are linked with the majority of diseases like aging, atherosclerosis, cancer, diabetes, liver cirrhosis, cardiovascular disorders, etc., [7]. The most common reactive oxygen species are superoxide anion ($O_2^{\cdot-}$), hydrogen peroxide (H_2O_2), peroxyl radical ($ROO^{\cdot}$) and highly reactive hydroxyl radical ($OH^{\cdot}$). The nitrogen derived free radicals are nitric oxide (NO) and peroxy nitrite anion ($ONOO^{\cdot}$). Oxidation process is one of the most important routes for producing free radicals in food, drugs and living systems. Antioxidants are the substances that when present in low concentration significantly delay or reduce the oxidation of the substrate [8].

BSA is made up of three homologous domains (I–III), which are divided into nine loops by 17 disulfide bridges. Each domain is composed of two sub-domains (A and B). Aromatic and heterocyclic ligands were found to bind within two hydrophobic pockets in sub-domain IIA and IIIA, site I and site II [9,10]. BSA has two tryptophans, Trp-134 and Trp-212, embedded in the first subdomain IB and sub-domain IIA, respectively. These changes appear to affect the secondary and tertiary structure of albumin. So, it is important to study the interaction of MBMPB with BSA, and hence become an important research field in chemistry, life sciences and clinical medicine. The molecular structure of MBMPB was given in Fig. 1. In the present research article, we have analyses the antioxidant property of MBMPB and the binding interaction of BSA with MBMPB.

2. Experimental

2.1. Materials and methods

All BSA solution were prepared in the Tris–HCl buffer solution (0.05 mol L^{-1} Tris, 0.15 mol L^{-1} NaCl, pH 7.4) and it was kept in the dark at 303 K. Tris base (2-amino-2-(hydroxymethyl)-1,3-propanediol) had a purity of not less than 99.5% and NaCl, HCl and other starting materials were all of analytical purity and doubly distilled water was used throughout.

2.2. In vitro antioxidant activity

2.2.1. DPPH radical scavenging activity

The stable free radical DPPH method is an easy, rapid and sensitive way to survey the antioxidant activity of a specific compound. The DPPH radical scavenging activity of MBMPB were determined by the reported method [11].

* Corresponding author. Tel.: +91 9443940735.
E-mail address: jtchalam2005@yahoo.co.in (J. Jayabharathi).

1011-1344/$ - see front matter © 2012 Elsevier B.V. All rights reserved.
http://dx.doi.org/10.1016/j.jphotobiol.2012.06.014

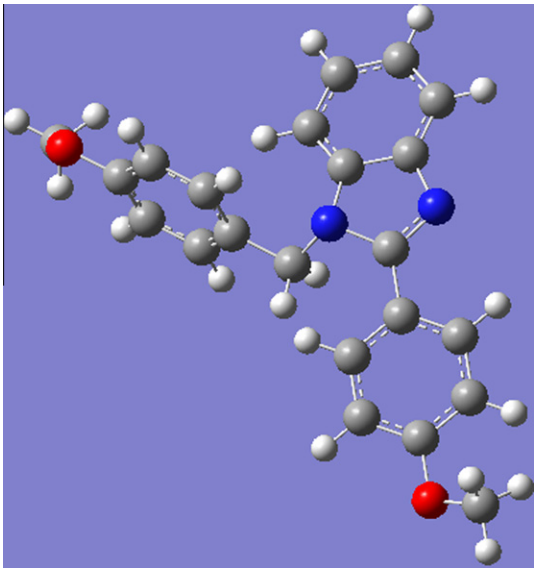

Fig. 1. Molecular structure of MBMPB.

2.2.2. Superoxide radical scavenging activity

Superoxide anion radical scavenging activity of MBMPB were determined by the reported method [12].

2.2.3. Hydroxyl radical scavenging activity

Hydroxyl radical scavenging activity of synthetic imidazole derivatives were determined by the reported method [13].

2.3. Optical measurements

NMR spectra have been recorded for the MBMPB on a Bruker 400 MHz instrument. The ultraviolet–visible (UV–vis) spectra have been measured on UV–vis spectrophotometer (Perkin Elmer, Lambda 35) and corrected for background due to solvent absorption. Photoluminescence (PL) spectra have been recorded on a (Perkin Elmer LS55) fluorescence spectrometer. Solvents used for spectral measurements are spectroscopic grade. Mass spectra have also been recorded on a Varian Saturn 2200 GCMS spectrometer.

2.4. Synthesis of 1-(4-methoxybenzyl)-2-(4-methoxyphenyl)-1H-benzo[d]imidazole

A mixture of 4-methoxybenzaldehyde (2 mmol), *o*-phenylenediamine (1 mmol) and ammonium acetate (2.5 mmol) has been refluxed at 80 °C in ethanol for appropriate time. The reaction was monitored by TLC and purified by column chromatography using petroleum ether: ethyl acetate (9:1) as the eluent. The ^{1}H NMR spectrum of MBMPB was given in Fig. 2 and ^{13}C NMR spectrum was given in Fig. 3. Yield: 60%. *mp* = 162 °C, Anal. calcd. for $C_{22}H_{20}N_2O_2$: C, 76.72; H, 5.85; N, 8.14; O, 9.29. Found: C, 77.02; H, 5.29; N, 8.33; O, 9.36. ^{1}H NMR (400 MHz, $CDCl_3$): δ 3.78 (s, 3H), 3.85 (s, 3H), 5.38 (s, 2H), 6.84–6.86 (d, 2H), 6.96–6.98 (d, 2H), 7.02–7.04 (d, 2H), 7.21–7.22 (d, 2H), 7.24–7.31 (m, 2H), 7.62–7.64 (d, 2H), 7.83–7.85 (s, 1H). ^{13}C (100 MHz, $CDCl_3$): δ 47.91 ($-CH_2$ carbon), 55.32, 55.40 (methoxy carbons), 110.43, 114.20, 114.44, 119.73, 122.47, 122.54, 122.75, 127.23, 128.51, 130.73, 136.11, 143.19, 154.15, 159.12, 160.91 (Aromatic carbons). MS: *m/e* 344.2, calcd 345.15[M + 1].

3. Results and discussion

3.1. FT-IR characteristics of MBMPB–BSA

Fourier transform infrared (FT-IR) technique was provided information about the nature of interaction between the MBMPB and BSA. Fig. 4a shows the FT-IR spectrum of MBMPB. Fig. 4b shows MBMPB bound to the BSA. The spectrum of pure MBMPB shows the >C=N stretching vibration at 1595 cm^{-1}. This band is

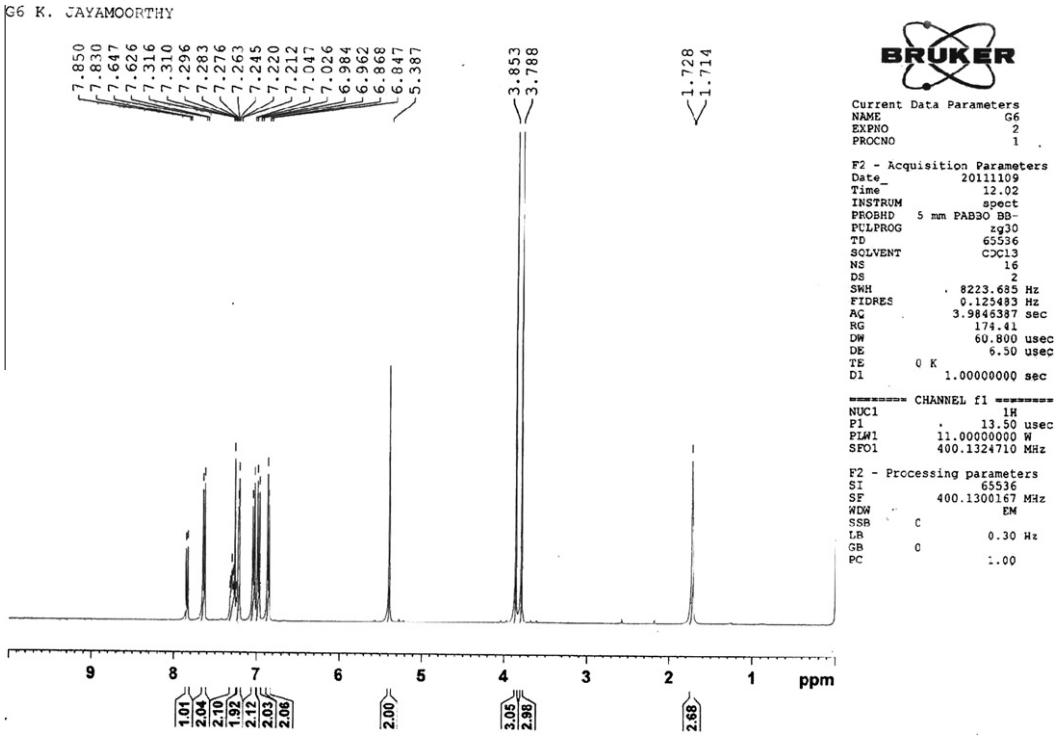

Fig. 2. ^{1}H NMR spectrum of MBMPB.

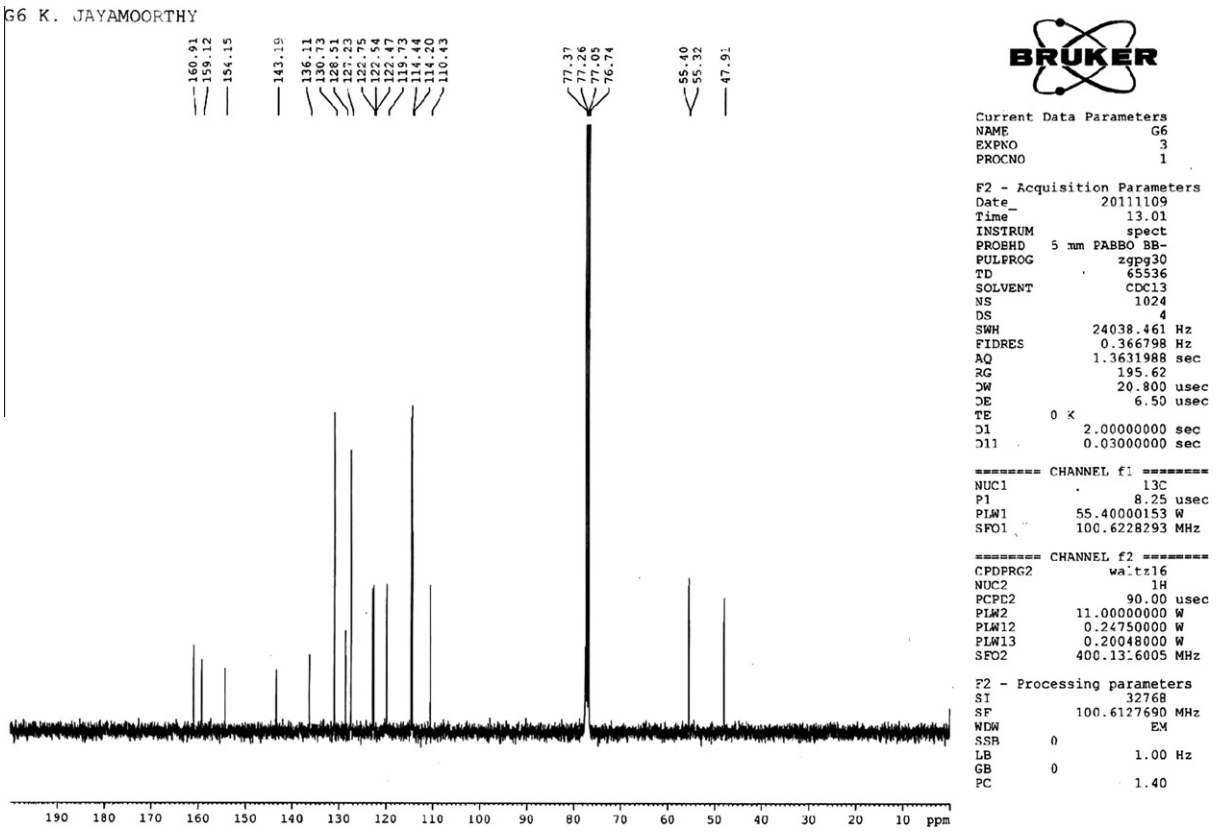

Fig. 3. ^{13}C NMR spectrum of MBMPB.

shifted from 1595 cm^{-1} to 1619 cm^{-1} for MBMPB bound to the BSA.

3.2. Fluorescence spectral studies

The interaction between MBMPB and BSA was investigated by evaluating fluorescence intensity on the BSA before and after the addition of the MBMPB. Here, the concentrations of BSA were stabilized at 1.0×10^{-5} mol L^{-1} and the concentration of MBMPB varied from 0 to 3.5×10^{-5} mol L^{-1} at increments of 0.5×10^{-5} mol L^{-1}. The effect of the MBMPB on BSA fluorescence intensity is shown in Fig. 5. The fluorescence intensity of BSA decreases progressively but the emission maximum did not move to shorter or longer wavelength, due to the interaction of MBMPB with BSA and quench its intrinsic fluorescence (Trp-212) [14], but there was no alteration in the local dielectric environment of BSA. Forster type fluorescence resonance energy transfer (FRET) mechanism (Fig. 6) is involved in the quenching of fluorescence by MBMPB in BSA–MBMPB complex. Therefore the possible quenching mechanism of fluorescence of BSA by MBMPB is not initiated by dynamic collision but from the formation of the BSA–MBMPB complex.

The quenching mechanism of MBMPB with BSA was probed using the Stern–Volmer equation [15], which can be applied to determine K_{SV} by linear regression from the Stern–Volmer plot of F_0/F against [MBMPB] (Fig. 7) at different temperatures. Table 1 summarizes the values of K_{sv} and K_A at different temperatures, which shows the values of Stern–Volmer quenching constant K_{sv} and K_A decreases with increase in temperature. According to the literature [16] for dynamic quenching, the maximum scatter collision quenching constant of various quenchers with the biopolymer is 2.0×10^{10} L mol^{-1} s^{-1} and the fluorescence lifetime of the biopolymer is 10^{-8} s. From Fig. 7, the values of K_{SV} and K_q ($=K_{SV}/\tau_0$) were calculated. The obtained values of K_q were larger than the limiting diffusion rate constant of the biomolecule (2.0×10^{10} L mol^{-1} s^{-1}), which indicate that the fluorescence quenching is caused by a specific interaction between BSA and MBMPB. Therefore, the quenching mechanism mainly arises from the formation of BSA–MBMPB complex rather than dynamic quenching. So it was implied that the static quenching was dominant in the system. From the plot of log $[(F_0 - F)/F]$ *vs* log [MBMPB], binding constants K_A and the number of binding sites '*n*' were calculated from the intercept and slope.

3.3. Determination of thermodynamic parameters

In order to elucidate the interaction between the MBMPB and BSA, the thermodynamic parameters were calculated from the van't Hoff plots. If the enthalpy change (ΔH) does not vary significantly over the temperature range studied then the thermodynamic parameters ΔH, ΔG and ΔS can be determined from the following equations respectively.

$$\ln K = \Delta H/RT + \Delta S/R \quad (1)$$

$$\Delta G = -RT \ln K \quad (2)$$

$$\Delta S = (\Delta H - \Delta G)/T \quad (3)$$

Table 2 shows the values of ΔH and ΔS obtained for the binding site from the van't Hoff plot. The negative sign for free energy (ΔG) shows that the binding process is spontaneous. The negative enthalpy (ΔH) and positive entropy (ΔS) values of the interaction of the MBMPB and BSA indicate that the specific electrostatic interactions played major role in the reaction [17].

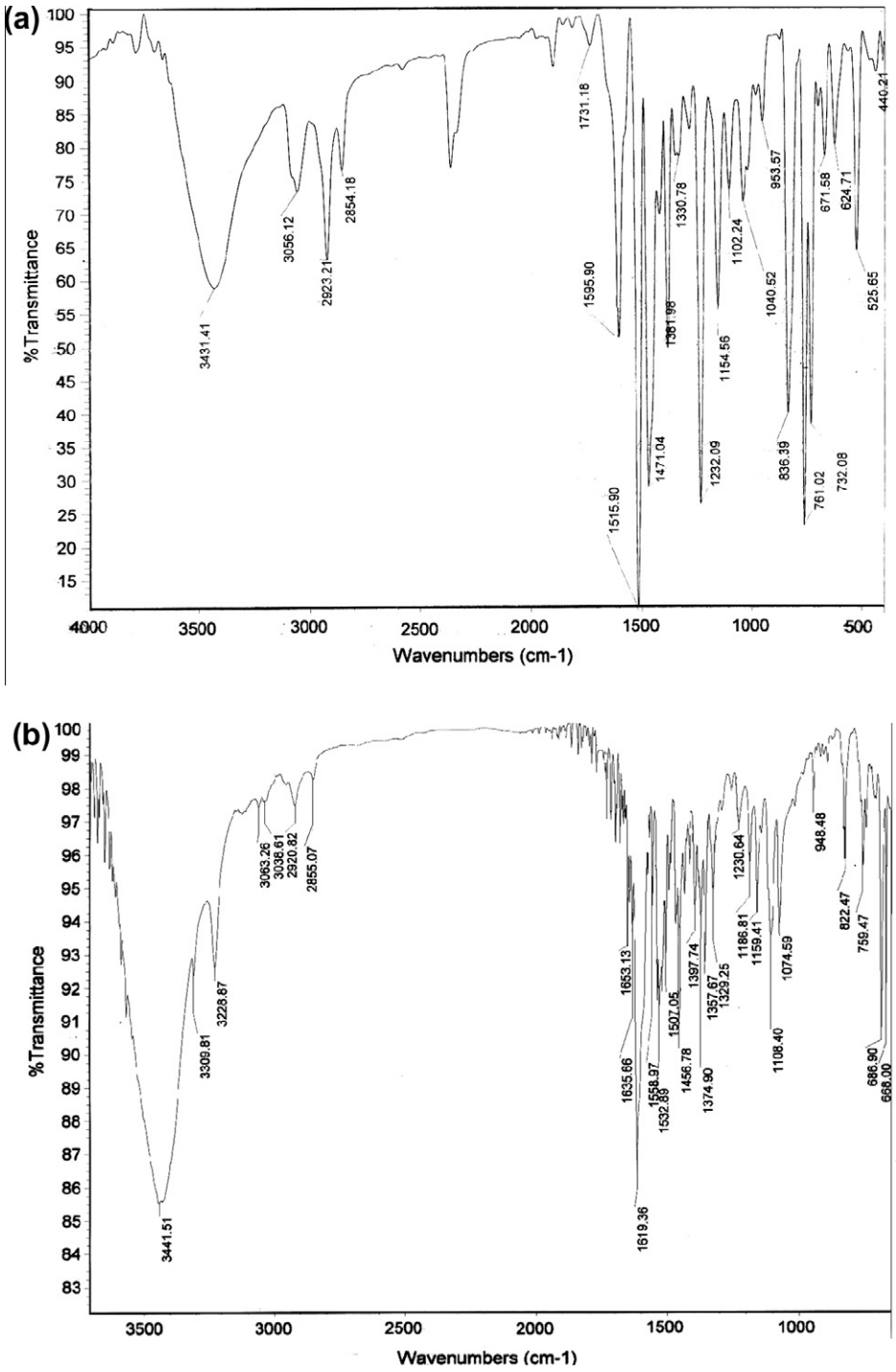

Fig. 4. (a) FT-IR spectrum of MBMPB (b) FT-IR spectrum of MBMPB bound with BSA.

3.4. Energy transfer from BSA to MBMPB

Energy transfer takes place through direct electro-dynamic interaction between the excited molecule and its neighbors [18]. The distance between the donor (BSA) and the acceptor (MBMPB) was estimated by Forster's non-radiative energy transfer theory and the overlapping of fluorescence spectra of BSA with absorption spectra of MBMPB was shown in Fig. 8. According to Forster's non-radiative energy transfer theory, the energy transfer efficiency (E) can be defined as the following equations:

$$E = 1 - (F/F_0) = R_0^6 \Big/ \left(R_0^6 + r_0^6\right) \tag{4}$$

$$R_0^6 = 8.8 \times 10^{-25}[\kappa^2 n^{-4} \Phi_D J(\lambda)] \text{ in Å} \tag{5}$$

$$J(\lambda) = \int_0^\infty F_D(\lambda)\varepsilon_A(\lambda)\lambda^4 d\lambda \tag{6}$$

where E is the efficiency of transfer between the donor and the acceptor, R_0 is the critical distance when the efficiency of transfer is 50%. F_D (λ) is the corrected fluorescence intensity of the donor at wavelength λ to ($\lambda + \Delta\lambda$), with the total intensity normalized to

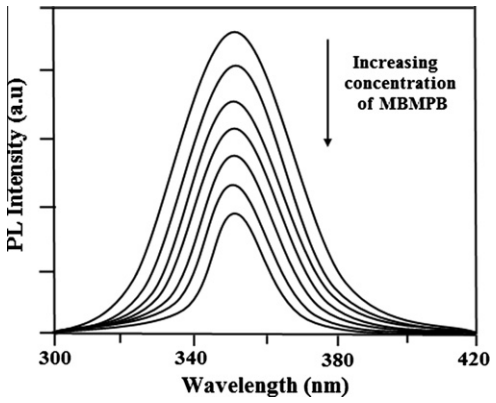

Fig. 5. Fluorescence quenching spectra of BSA at different concentrations of MBMPB.

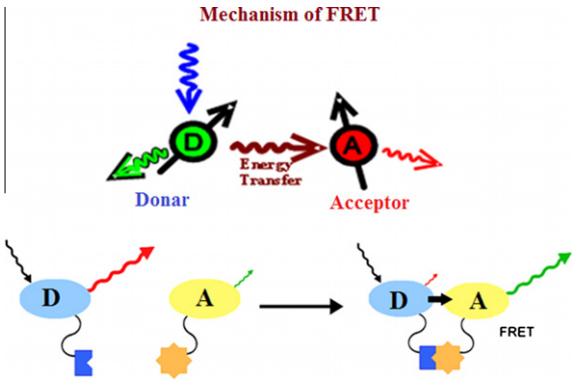

Fig. 6. Fluorescence resonance energy transfer (FRET) mechanism.

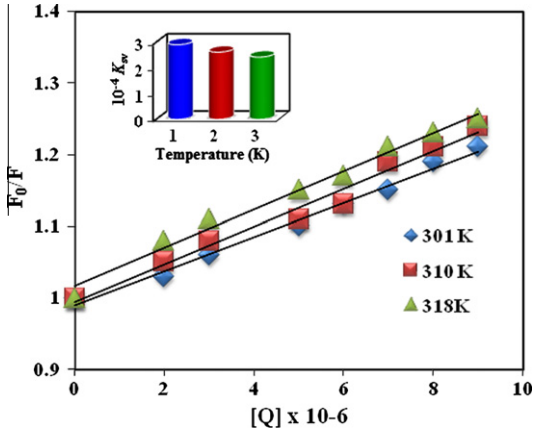

Fig. 7. Stern–Volmer plot of F_0/F against [MBMPB].

Table 1
K_{sv} K_A, n and r values of BSA–MBMPB system at 301, 310 and 318 K.

T (K)	K_{sv} (10^4 L mol^{-1})	K_A (10^4 L mol^{-1})	n	r
301	2.9	3.71	1.23	0.99
310	2.61	2.69	1.04	0.99
318	2.42	2.12	1.00	0.99

unity and $\varepsilon_A(\lambda)$ is the molar extinction coefficient of the acceptor at wavelength λ. The Forster distance (R_0) has been calculated

Table 2
Thermodynamic parameters of BSA–MBMPB system at 301, 310 and 318 K.

T (K)	ΔH (kJ mol^{-1})	ΔG (kJ mol^{-1})	ΔS (J mol^{-1} K^{-1})
301	−27.67	−23.55	6.48
310		−24.70	
318		−23.10	

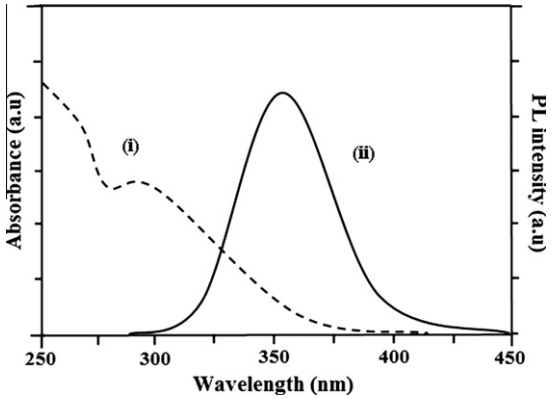

Fig. 8. Overlapping fluorescence spectra of BSA (i) with absorption spectra of MBMPB (ii).

assuming random orientation of the donor and acceptor molecules. Here, $\kappa^2 = 2/3$, $n = 1.311$, $\Phi_D = 0.20$ and from the available data, it results that $J(\lambda) = 4.07 \times 10^{-12}$ cm^3 L mol^{-1}, $E = 0.30$, $R_0 = 0.70$ nm and $r = 0.89$ nm. The donor-to-acceptor distance is less than 8 nm which indicates that the energy could transfer from BSA to MBMPB [19] with high probability and the distance obtained by FRET with higher accuracy.

3.5. Conformation investigation

To exploit the structural change of BSA by addition of the MBMPB, we have measured synchronous fluorescence spectra of BSA with various amounts of MBMPB. The synchronous fluorescence spectra [20] of BSA with various amount of MBMPB were recorded at $\Delta\lambda = 15$ nm and $\Delta\lambda = 60$ nm (Fig. 9a and b). It is apparent from the figure that the emission wavelength of the tyrosine residues is blue-shifted (λ_{max} from 353 to 340 nm in Fig. 9a) with increasing concentration of MBMPB. This blue shift expressed that the conformation of BSA was changed and it suggested a less polar (or more hydrophobic) environment of tyrosine residue [21]. At the same time, the tryptophan fluorescence emission is decreased regularly, but no significant change in wavelength was observed. It suggests that the interaction of MBMPB with BSA does not affect the conformation of tryptophan micro-region. The tyrosine fluorescence spectrum may represent that the conformation of BSA is somewhat changed, due to the blue shift (Fig. 9a), leading to the polarity around *Tyr* residues was decreased and the hydrophobicity was increased [22], but the interaction of MBMPB with BSA does not obviously affect the conformation of tryptophan micro-region [23]. The MBMPB could involve the second site (sub-domain IB) with higher binding affinity and the formation of complex led to the observation of the blue shift of tyrosine residues fluorescence. This is because the tyrosine contains one aromatic hydroxyl group unlike tryptophan and tyrosine can undergo an excited state ionization, resulting in the loss of the proton on the aromatic hydroxyl group. The hydroxyl group can dissociate during the lifetime of its excited state, leading to quenching. Hence the aromatic hydroxyl

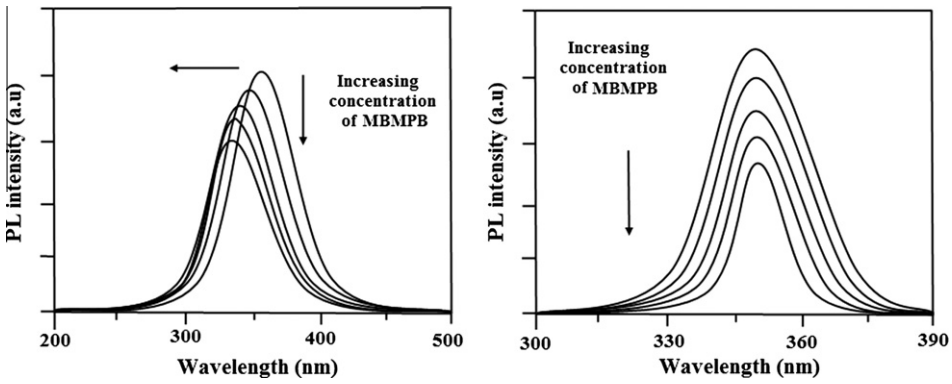

Fig. 9. Synchronous fluorescence spectra of BSA in the presence and absence of MBMPB (a) at $\Delta\lambda$ = 15 nm and (b) at $\Delta\lambda$ = 60 nm.

group present in the tyrosine residues is responsible for the interaction of BSA with MBMPB.

For reconfirming the structural change of BSA by the addition of the MBMPB, we have measured the UV–vis absorbance spectra of BSA with various amounts of the MBMPB. Fig. 10 displays the UV–vis absorbance spectra of BSA at different concentrations of the MBMPB. The absorption band of 210 nm of BSA is characteristic of α–helix structure of BSA. The intensity of absorbance of BSA was decreased with increasing concentration of the MBMPB and the peak was red shifted. In addition, the absorption peaks in the UV–vis spectra at approximately 290 nm rise gradually (from curve (a) to curve (e)) and blue shifted to about 11 nm with increasing concentration of the MBMPB. These results indicating that the interaction between the MBMPB and BSA and the fluorescence quenching of BSA by MBMPB was the result of the formation of BSA–MBMPB complex [24]. These results confirmed that the quenching was mainly a static quenching process.

3.6. In vitro antioxidant activity

3.6.1. DPPH radical scavenging activity

MBMPB, at various concentrations ranging from 10, 20, 40, 60, 80 and 100 μM, were mixed in 1 mL of freshly prepared 0.5 mM DPPH ethanolic solution and 2 mL of 0.1 M acetate buffer at pH 5.5. The resulting solutions were then incubated at 37 °C for 30 min and measured at 517 nm in a Shimadzu UV-1601 spectrophotometer. DPPH· scavenging activities of the MBMPB were calculated from the decrease in absorbance from 517 nm in comparison with the negative control (Fig. 11).

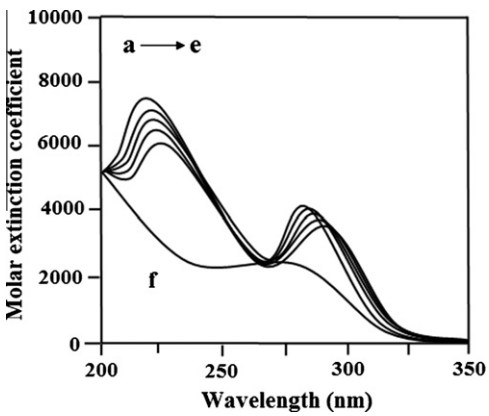

Fig. 10. Absorption spectra of BSA in the presence of MBMPB (a–e) and in the absence of MBMPB (f).

$$\%\ \text{of DPPH}^{\cdot}\ \text{scavenging} = [A_0 - A_1/A_0] \times 100 \quad (7)$$

where A_0 was the absorbance of the control and A_1 was the absorbance in the presence of the sample of MBMPB. MBMPB shows DPPH radical quenching activity in a concentration dependent manner.

3.6.2. Superoxide anion scavenging assay

It is well known that superoxide anions damage biomacromolecules directly or indirectly by forming H_2O_2, OH·, peroxylnitrite, or singlet oxygen during pathophysiologic events such as ischemic-reperfusion injury. PMS_{red} (phenazine methosulphate) convert oxidized nitro blue tetrazolium (NBT_{oxi}) to the reduced form (NBT_{red}), which formed a violet colored complex. The color formation indicates the generation of superoxide anion, which was measured spectrophotometrically at 560 nm. A decrease in the formation of color after addition of the antioxidant was a measure of its superoxide scavenging activity.

The superoxide radical scavenging activities of MBMPB were evaluated based on their ability to quench the superoxide radical generated from the PMS/NADH reaction. 1 mL of NBT (100 μmol of NBT in 100 mM phosphate buffer, pH 7.4), 1 mL of NADH (468 μmol in 100 mM phosphate buffer, pH 7.4) solution and varying volume of imidazoles (10,20,40,60,80 and 100 μM) were mixed well. The reaction was started by the addition of 100 μl of PMS (60 μmol/100 mM phosphate buffer, pH 7.4). The reaction mixture was incubated at 30 °C for 15 min. The absorbance was measured at 560 nm in a spectrophotometer. Incubation without the compound was used as blank. Decreased absorbance of the reaction mixture indicates increased superoxide anion scavenging activity (Fig. 12). The percentage scavenging was calculated as follows:

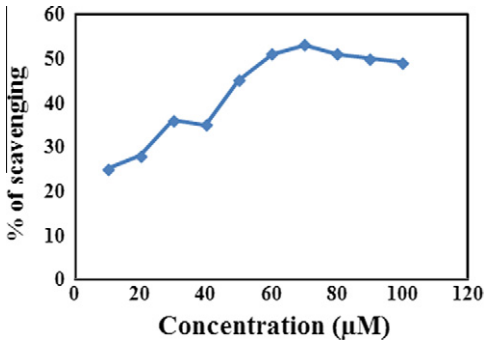

Fig. 11. Radical scavenging potential of MBMPB by DPPH method at different concentrations (μg/mL).

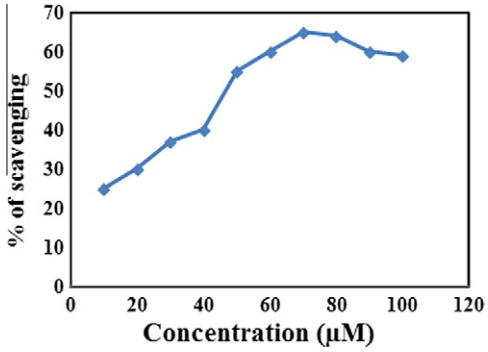

Fig. 12. Scavenging potential of MBMPB at different concentrations (μg/mL) on superoxide radicals generated by the PMS/NADH system.

$$\%\ \text{of scavenging}\ [O_2^{\cdot-}] = [A_0 - A_1/A_0] \times 100 \quad (8)$$

where A_0 was the absorbance of the control and A_1 was the absorbance in the presence of the sample of MBMPB. MBMPB shows Superoxide anion quenching activity in a concentration dependent manner.

3.6.3. Hydroxyl radical scavenging

In this assay, hydroxyl radical was produced by reduction of H_2O_2 by the transition metal (iron) in the presence of ascorbic acid. The generation of OH· is detected by its ability to degrade deoxyribose to form products, which on heating with thiobarbituric acid (TBA) form a pink color chromogen. Addition of MBMPB with deoxyribose for OH· and diminishes the color formation. The incubation mixture in a total volume of 1 mL contained 0.1 mL of buffer, varying volumes of MBMPB (10,20,40,60,80 and 100 μM), 0.2 mL of 500 μM ferric chloride, 0.1 mL of 1 mM ascorbic acid, 0.1 L of 1 M EDTA, 0.1 mL of 10 mM H_2O_2 and 0.2 mL of 2-deoxyribose. The contents were mixed thoroughly and incubated at room temperature for 60 min. Then, 1 mL of 1% TBA (1 g in 100 mL of 0.05 N NaOH) and 1 mL of 28% trichloroacetic acid (TCA) were added. All the tubes were kept in a boiling water bath for 30 min. The absorbance of the supernatant was observed at 535 nm with reagent blank containing water in place of compound. Decreased absorbance of the reaction mixture indicates increased hydroxyl radical scavenging activity (Fig. 13). The percentage scavenging was calculated as follows:

$$\%\ \text{of scavenging}\ [OH^{\cdot}] = [A_0 - A_1/A_0] \times 100 \quad (9)$$

where A_0 was the absorbance of the control and A_1 was the absorbance in the presence of MBMPB. MBMPB shows Hydroxyl radical quenching activity in a concentration dependent manner.

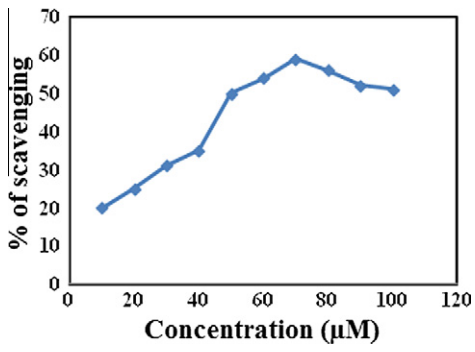

Fig. 13. Hydroxy radical scavenging potential of MBMPB at different concentrations (μg/mL) on deoxyribose degradation method.

4. Conclusion

In this article, we investigated the interaction of 1-(4-Methoxybenzyl)-2-(4-methoxyphenyl)-1H-benzo[d]imidazole (MBMPB) with bovine serum albumin (BSA) by solution spectral studies. The experimental results of fluorescence showed that the quenching of BSA by MBMPB is a result of the formation of BSA–MBMPB complex; static quenching and non-radiative energy transferring were confirmed to result in the fluorescence quenching. Binding reaction is play major role in the reaction is showed by thermodynamic parameters. Synchronous fluorescence spectrum shows the interaction of the MBMPB with BSA affects the conformation of tyrosine residues micro-region. MBMPB shows potential antioxidant property due to the couple of electron releasing methoxy group.

Acknowledgments

One of the authors Prof. J. Jayabharathi is thankful to Department of Science and Technology [No. SR/S1/IC-73/2010], University Grants commission (F. No. 36-21/2008 (SR)) and Defence Research and Development Organisation (DRDO) (NRB-213/MAT/10-11) for providing funds to this research study.

References

[1] Z. Fang, S. Wang, L. Zhao, Z. Xu, J. Ren, X. Wang, A novel polymerizable imidazole derivative for blue light-emitting material, Mater. Lett. 61 (2007) 4803–4807.
[2] Z. Ge, T. Hayakawa, S. Ando, M. Ueda, T. Akiike, H. Miyamoto, Solution-processible bipolar triphenylamine-benzimidazole derivatives for highly efficient single-layer organic light-emitting diodes, Chem. Mater. 20 (2008) 2532–2537.
[3] M.Y. Lai, C.H. Chen, W.S. Huang, J.T. Lin, T.H. Ke, L.Y. Chen, Benzimidazole/amine-based compound capable of ambipolar transport for application in single-layer blue-emitting oleds and as hosts for phosphorescent emitters, Angew. Chem. Int. Ed. 47 (2008) 581–585.
[4] R.Y.C. Shin, T. Kietzke, S. Sudhakar, A. Dodabalapur, Z.K. Chen, A. Sellinger, Ntype conjugated materials based on 2-vinyl-4,5-dicyanoimidazoles and their use in solar cells, Chem. Mater. 19 (2007) 1892–1894.
[5] M.S. Tsai, Y.C. Hsu, J.T. Lin, H.C. Chen, C.-P. Hsu, Organic dyes containing 1hphenanthro[9,10-d]imidazole conjugation for solar cells, J. Phys. Chem. C 111 (2007) 18785–18793.
[6] A. Mallick, S.C. Bera, S. Maiti, N. Chattopadhya, Fluorometric investigation of interaction of 3-acetyl-4-oxo-6,7-dihydro-12H indolo-[2,3-a] quinolizine with bovine serum albumin, Biophys. Chem. 112 (2004) 9–14.
[7] J.M.C. Gutteridgde, Free radicals in disease processes: a complication of cause and consequence, Free Radic. Res. Comm. 19 (1995) 141–158.
[8] B. Halliwell, The antioxidant paradox, Lancet 355 (2000) 1179–1180.
[9] Y. Li, W.Y. He, H.X. Liu, X.J. Yao, Z.D. Hu, Daidzein interaction with human serum albumin studied using optical spectroscopy and molecular modeling methods, J. Mol. Struct. 831 (2007) 144–150.
[10] P. Sevilla, J.M. Rivas, F. García-Blanco, J.V. García-Ramos, S. Sánchez-Cortés, Identification of the anti tumoral drug emodin binding sites in bovine serum albumin by spectroscopic methods, Biochim. Biophys. Acta 1774 (11) (2007) 1359–1369.
[11] D. Baricevic, S. Sosa, R. Della Loggia, A. Tubaro, B. Simonovska, A. Krasna, A. Zupancic, Topical anti-inflammatory activity of *salvia officinalis* L. leaves: the relevance of ursolic acid, J. Ethnopharmacol. 75 (2001) 125–132.
[12] M. Nishimiki, N.A. Rao, K. Yagi, The occurrence of superoxide anion in the reaction of reduced phenazine methosulphate and molecular oxygen, Biochem. Biophys. Res. Comm. 46 (1972) 849–853.
[13] K. Elizabeth, M.N.A. Rao, Oxygen radical scavenging activity of curcumin, Int. J. Pharm. 58 (1990) 237–240.
[14] J. Jayabharathi, V. Thanikachalam, M. Venkatesh Perumal, N. Srinivasan, Fluorescence resonance energy transfer from a bio-active imidazole derivative 2-(1-phenyl-1H-imidazo[4,5-f][1,10]phenanthrolin-2-yl)phenol to a bioactive indoloquinolizine system, Spectrochim. Acta A 79 (2011) 236–244.
[15] J.R. Lakowicz, Principles of Fluorescence Spectroscopy, third ed., Springer, New York, 2006.
[16] H. Cao, D. Wu, H. Wang, M. Xu, Effect of the glycosylation of flavonoids on interaction with protein, Spectrochim. Acta A 73 (2009) 972–975.
[17] S.N. Timaseff, Thermodynamis of protein interactions, in: H. Pecters (Ed.), Proteins of Biological Fluids, Pergamon Press, Oxford, 1972, pp. 511–519.
[18] T. Forster, Intermolecular energy migration and fluorescence, Ann. Phys. 2 (1948) 55–75.

[19] M.M. Yang, X.L. Xi, P. Yang, Study of the interaction of cephalosporin class medicine with albumin by fluorescence enhancement and fluorescence quenching theories, Chin. J. Chem. 24 (2006) 642–648.
[20] J. Jayabharathi, V. Thanikachalam, M. Venkatesh Perumal, Mechanistic investigation on binding interaction of bioactive imidazole with protein bovine serum albumin-A biophysical study, Spectrochim. Acta A 79 (2011) 502–507.
[21] Y.J. Hu, Y. Liu, W. Jiang, R.M. Zhao, S.S. Qu, Fluorometric investigation of the interaction of bovine serum albumin with surfactants and 6-mercaptopurine, J. Photochem. Photobiol. B: Biol. 80 (2005) 235–242.
[22] J.H. Tang, F. Luan, X.G. Chen, Binding analysis of glycyrrhetinic acid to human serum albumin: fluorescence spectroscopy, FTIR, and molecular modeling, Bioorg. Med. Chem. 14 (2006) 3210–3217.
[23] W.C. Abert, W.M. Gregory, G.S. Allan, The binding interaction of coomassie blue and proteins, Anal. Biochem. 213 (1993) 407–413.
[24] Q. Sun, Z. Li, X. Zeng, M. Ge, D. Wang, Structures and properties of the hydrogen-bond complexes: theoretical studies for the coupling modes of the pyrazole–imidazole system, J. Mol. Struct. (Theochem) 724 (2005) 167–172.